

# Dynamic stress analysis of a functionally graded material plate with a circular hole

Quanquan Yang · Cun-Fa Gao

Received: 2 October 2011 / Accepted: 31 July 2012 / Published online: 15 August 2012  
© Springer Science+Business Media B.V. 2012

**Abstract** This paper is to study the two-dimensional dynamic stress of a functionally graded material (FGM) plate with a circular hole under plane compressional waves at infinity. With using the method of piece-wise homogeneous layers, the dynamic stress distribution of the FGM plate having radial arbitrary material parameters is derived based on the complex variable method. As examples, numerical results are presented for the FGM plate having given radial shear modulus, density and Poisson's ratio. It is found that the dynamic stress around the circular hole in the FGM plate can be effectively reduced by choosing the proper change ways of the radial material parameters for different frequency incident wave.

**Keywords** Functionally graded material · Circular hole · Dynamic stress

## 1 Introduction

Functionally graded materials (FGMs) are composites in which the material properties vary continuously as a known function along a direction. The continuous

change in microstructure of FGMs avoids the mismatch of material properties across the interface, and thus stress concentration can be effectively reduced compared with that in the case where there are material interfaces. Especially, when the structures are subjected to dynamic loading, the stresses can be decreased by choosing the proper change ways of the radial material properties. Thus, it is of great importance to study dynamic stresses in FGMs.

In the past decade, a lot of works have been done in the study of the dynamic stress around and near the discontinuities in FGMs. Ma *et al.* [1] studied the dynamic behavior of two collinear cracks in FGM layer bonded to dissimilar half planes under anti-plane shear waves by the Schmidt method. Meguid *et al.* [2] analyzed the singularity behavior of a crack propagating in an infinite medium with spatially varying elastic properties under plane elastic deformation. Using Laplace and Fourier transforms, Chen *et al.* [3] investigated the transient response of an infinite functionally graded piezoelectric medium containing a through crack subjected to electromechanical impact. Song and Paulino [4] obtained the dynamic stress intensity factors for homogeneous and smoothly heterogeneous materials using the interaction integral method. Feng and Su [5] investigated the dynamic anti-plane problem for a functionally graded magneto-electro-elastic strip containing an internal crack perpendicular to the boundary. Li and Lee [6] dealt with the dynamic fracture behavior of a weak-discontinuous interface in a symmetrical functionally gradient composite

---

Q. Yang · C.-F. Gao (✉)  
State Key Laboratory of Mechanics and Control of  
Mechanical Structures, Nanjing University of Aeronautics  
& Astronautics, Nanjing 210016, China  
e-mail: [cfgao@nuaa.edu.cn](mailto:cfgao@nuaa.edu.cn)

strip loaded by anti-plane impact. Peng and Li [7] analyzed the dynamic magneto-electroelastic of a homogeneous magneto-electroelastic substrate with a functionally graded coating containing a crack at the interface. Han *et al.* [8] presented an analytical-numerical method for analyzing characteristics of waves in a cylinder composed of FGM. Chen *et al.* [9] investigated the free vibration of an arbitrarily thick orthotropic piezoelectric hollow cylinder with a functionally graded property along the thickness direction and filled with a non-viscous compressible fluid medium. Elmaimouni *et al.* [10] numerically calculated the guided wave propagation in an infinite cylinder composed of FGM. Based on the Green-Lindsay theory, Bagri and Eslami [11] analyzed the thermoelastic waves in functionally graded hollow spheres. Asgari *et al.* [12] considered two-dimensional functionally graded thick hollow cylinder with finite length subjected to impact internal pressure. Shariyat *et al.* [13] studied nonlinear thermo-elasticity, vibration, and stress wave propagation analyses of thick FGM cylinders with temperature-dependent material properties.

However, previous works cited above are mainly restricted to the case of a FGM plate with cracks or a FGM hollow cylinder, and not much work can be found for the analysis of dynamic stress concentrations around a hole or cavity in functionally graded materials, although a number of works on dynamic stress concentrations around the hole or cavity have been reported for the case of homogeneous materials. For example, earlier work on dynamic stress concentrations in homogeneous materials has been given by Pao [14], who discussed the dynamical stress concentration around a circular hole in an infinitely elastic plate during passage of plane compressional waves. Shortly thereafter, Mow and McCabe [15] studied the dynamic stresses in an arbitrarily thick elastic cylinder in an infinite elastic medium under plane, compressional, harmonically time-varying waves. Later, Liu *et al.* [16] presented a complex function method for analyzing the dynamic stress concentrations around the circular and elliptical cavities. Shankar [17] investigated the behavior of dynamic stress in a flat plate with a square hole by using statistical energy analysis methods. Altenhof *et al.* [18] considered the dynamic stress concentrations for an axially loaded strut at discontinuities due to an elliptical hole or double circular notches. Zirka *et al.* [19] experimentally studied the dynamic stress concentration factor near a hole in an

orthotropic plate by photoelastic method. Using dual reciprocity boundary element method, Gao *et al.* [20] analyzed the scattering of elastic waves and dynamic stress concentrations in the thin plate with cutout. Wang *et al.* [21] dealt with the dynamic stress concentration around elliptic cavities in saturated poroelastic soil under harmonic plane waves with complex variable method. Wang *et al.* [22] investigated the diffraction of plane harmonic compressional wave and the dynamics stress concentration in a solid with a nano-sized circular hole.

Recently, some works have been made on dynamic stress concentrations in a FGM plane with a hole or cavity. For example, Fang *et al.* [23–25] presented a theoretical method to investigate the multiple scattering of shear waves and dynamic stress concentrations in semi-infinite FGM and semi-infinite slab of FGM with a circular cavity. More recently, Dineva *et al.* [26] calculated the stress and electric field concentrations around a circular hole in a functionally graded piezoelectric plane subjected to anti-plane elastic SH-wave and in-plane time-harmonic electric load. However, in the above works [23–26], it is all assumed that the material parameters vary along the thickness direction.

In the present work, we present a complex variable method for calculating the dynamic stress concentrations around a circular hole in a FGM plate in which the material properties are graded in the radial direction. Following the Introduction, basic equations of two dimensional elastic problems are outlined for later use in Sect. 2. In Sect. 3, theoretical analysis is done for the FGM plate with a circular hole subjected to plane compressional waves at infinity based on the method of piece-wise homogeneous layers. Then, numerical examples are given to discuss the effect of varying the shear modulus  $\mu$ , density  $\rho$  and the Poisson's ratio  $\nu$  on the dynamic stress around the hole in Sect. 4. Finally, Sect. 5 concludes the present work.

## 2 Basic equations

Consider the two-dimensional problem of an isotropic and homogeneous solid in a fixed rectangular coordinate system  $(x - y)$ . The equations of motion for the displacements in the directions of  $x$  and  $y$  axes respectively,  $u$  and  $v$ , are:

$$\mu \nabla^2 u + (\lambda + \mu) \frac{\partial \theta}{\partial x} = \rho \frac{\partial^2 u}{\partial t^2}, \quad (1)$$

$$\mu \nabla^2 v + (\lambda + \mu) \frac{\partial \theta}{\partial y} = \rho \frac{\partial^2 v}{\partial t^2}, \tag{2}$$

where,  $\lambda$  and  $\mu$  are the Lamé elastic constants and  $\rho$  is the density of the medium;  $\nabla^2$  indicates Laplace operator; and  $\theta$  is the two dimensional dilatation:

$$\theta = \frac{\partial u}{\partial x} + \frac{\partial v}{\partial y}. \tag{3}$$

The wave potentials,  $\Phi$  and  $\Psi$ , are related to  $u$  and  $v$  as follows:

$$u = \frac{\partial \Phi}{\partial x} + \frac{\partial \Psi}{\partial y}, \tag{4}$$

$$v = \frac{\partial \Phi}{\partial y} - \frac{\partial \Psi}{\partial x}. \tag{5}$$

The equations of motion are satisfied provided that  $\Phi$  and  $\Psi$  are the solutions of the following wave equations:

$$\nabla^2 \Phi = \frac{1}{c_p^2} \frac{\partial^2 \Phi}{\partial t^2}, \tag{6}$$

$$\nabla^2 \Psi = \frac{1}{c_s^2} \frac{\partial^2 \Psi}{\partial t^2}. \tag{7}$$

In the above,  $c_p = [(\lambda + 2\mu)/\rho]^{1/2}$  and  $c_s = (\mu/\rho)^{1/2}$  are propagation velocities of compressive and shear waves in the medium, respectively.

Using the complex variable method introduced by Liu *et al.* [16], Eqs. (6) and (7) in complex-plane ( $z, \bar{z}$ ) can be expressed as:

$$4 \frac{\partial^2 \Phi}{\partial z \partial \bar{z}} = \frac{1}{c_p^2} \frac{\partial^2 \Phi}{\partial t^2}, \tag{8}$$

$$4 \frac{\partial^2 \Psi}{\partial z \partial \bar{z}} = \frac{1}{c_s^2} \frac{\partial^2 \Psi}{\partial t^2}, \tag{9}$$

where  $z = x + iy = r \cdot e^{i\theta}$  and  $\bar{z} = x - iy = r \cdot e^{-i\theta}$ .

In our study of the steady state waves,  $\Phi$  and  $\Psi$  can be expressed as:

$$\Phi(z, \bar{z}, t) = \text{Re} \varphi(z, \bar{z}) e^{-i\omega t}, \tag{10}$$

$$\Psi(z, \bar{z}, t) = \text{Re} \psi(z, \bar{z}) e^{-i\omega t}, \tag{11}$$

where  $\varphi(z, \bar{z})$  and  $\psi(z, \bar{z})$  are functions of  $z$  and  $\bar{z}$ ;  $\omega$  is the circular frequency of wave function.

Substituting Eqs. (10) and (11) into (8) and (9) results in:

$$\frac{\partial^2 \varphi}{\partial z \partial \bar{z}} = \left(\frac{i\alpha}{2}\right)^2 \varphi, \tag{12}$$

$$\frac{\partial^2 \psi}{\partial z \partial \bar{z}} = \left(\frac{i\beta}{2}\right)^2 \psi, \tag{13}$$

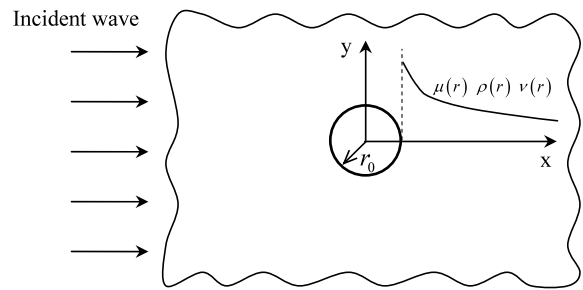


**Fig. 1** FGM plate with a circular hole subjected to plane compressional waves at infinity

where  $\alpha = \omega/c_p$  and  $\beta = \omega/c_s$  are the wave numbers of the compressional and shear waves. Expressions (12) and (13) are recognized as the spatial equations of wave functions in complex-plane. The corresponding stress expression can be written in the following form [16]:

$$\sigma_\theta + \sigma_r = -2\alpha^2(\lambda + \mu)\Phi(z), \tag{14}$$

$$\sigma_\theta - \sigma_r + 2i\tau_{r\theta} = -8\mu \frac{\partial^2}{\partial z^2} [\Phi(z) + i\Psi(z)] e^{2i\theta}, \tag{15}$$

where  $\sigma_r$ ,  $\sigma_\theta$  and  $\tau_{r\theta}$  are the components of stresses, respectively;  $\Phi(z)$  and  $\Psi(z)$  stand for the potential functions, and they can be determined by the following stress boundary condition:

$$\begin{aligned} -\alpha^2(\lambda + \mu)\Phi(z) + 4\mu \frac{\partial^2}{\partial z^2} [\Phi(z) + i\Psi(z)] e^{2i\theta} \\ = F_1 - iF_2, \end{aligned} \tag{16}$$

or displacement boundary condition:

$$2 \frac{\partial}{\partial \bar{z}} [\Phi(z) - i\Psi(z)] e^{-i\theta} = u_r + iv_\theta, \tag{17}$$

where  $F_1$ ,  $F_2$ ,  $u_r$  and  $v_\theta$  represent the components of force and displacement at the boundary, respectively.

### 3 Theoretical analysis

Consider a FGM plate with a free circular hole, as shown in Fig. 1. It is assumed that all the material constants in the plane vary only along the radial direction, and the plate is subjected to plane compressional waves at infinity. In this case, the method of piece-wise homogeneous layers can be used, that is, the plate can be decomposed to  $N$  inner rings  $S^{(1)}, S^{(2)}, \dots, S^{(i)}, \dots, S^{(N)}$  with equal thickness, and

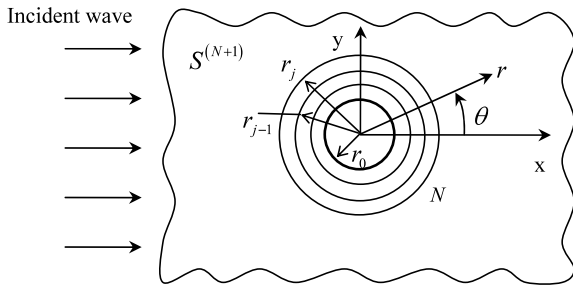


Fig. 2 Decomposing the plate into  $N$  rings

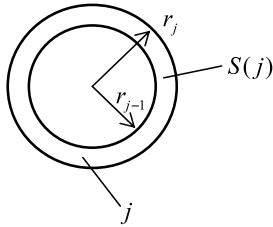


Fig. 3 Any ring No.  $j$

an outer region  $S^{(N+1)}$ , as shown in Fig. 2 where the material constants in any ring can be regards as unchanged.

The incident plane compressional waves, Fig. 1, are represented by:

$$\Phi^{(i)} = \varphi_0 e^{i(\alpha x - \omega t)}, \tag{18}$$

$$\Psi^{(i)} = 0, \tag{19}$$

where  $\varphi_0$  is the amplitude of the incident wave and  $\alpha = \alpha_{N+1} = \omega / c_{p(N+1)}$  is the wave number in region  $S^{(N+1)}$ .

By applying Jacobi-Anger identity,  $\Phi^{(i)}$  can be expressed as:

$$\Phi^{(i)} = \varphi_0 \sum_{-\infty}^{\infty} i^n J_n(\alpha r) e^{in\theta} e^{-i\omega t}, \tag{20}$$

in which  $J_n$  denotes the Bessel function of order  $n$ .

Inside any inner ring  $S^{(j)}$  ( $j = 1, 2, \dots, N$ ), as shown in Fig. 3, the complex potentials can be expressed as:

$$\varphi_j(z) = \sum_{-\infty}^{\infty} [a_n^{(j)} H_n^1(\alpha_j r) + c_n^{(j)} H_n^2(\alpha_j r)] e^{in\theta}, \tag{21}$$

$$\psi_j(z) = \sum_{-\infty}^{\infty} [b_n^{(j)} H_n^1(\beta_j r) + d_n^{(j)} H_n^2(\beta_j r)] e^{in\theta}, \tag{22}$$

where  $j = 1, 2, \dots, N$ ,  $a_n^{(j)}, b_n^{(j)}, c_n^{(j)}, d_n^{(j)}$  are unknown coefficient;  $H_n^1, H_n^2$  denote the Hankel function of the first and second kind of order  $n$ , respectively.

Inside the outer region  $S^{(N+1)}$ , the complex potentials can be expressed as:

$$\varphi_{N+1}(z) = \sum_{-\infty}^{\infty} [a_n^{(N+1)} H_n^1(\alpha_{N+1} r) + \varphi_0 i^n J_n(\alpha_{N+1} r)] e^{in\theta}, \tag{23}$$

$$\psi_{N+1}(z) = \sum_{-\infty}^{\infty} [b_n^{(N+1)} H_n^1(\beta_{N+1} r)] e^{in\theta}, \tag{24}$$

where  $a_n^{(N+1)}, b_n^{(N+1)}$  are unknown coefficients.

On the surface of the hole, one has  $F_1 = F_2 = 0$ , and this condition requires from Eq. (16) that:

$$-\alpha_1^2 (\lambda_1 + \mu_1) \Phi_1(z) + 4\mu_1 \frac{\partial^2}{\partial z^2} [\Phi_1(z) + i\Psi_1(z)] e^{2i\theta} = 0, \tag{25}$$

where  $z = r_0 \sigma = r_0 e^{i\theta}$ .

Substituting Eqs. (21) and (22) into (25), and multiplying  $e^{-is\theta}$  at both sides of the equations, then integrating from  $-\pi$  to  $\pi$ , one has:

$$[-\alpha_1^2 (\lambda_1 + \mu_1) H_n^1(\alpha_1 r_0) + \mu_1 \alpha_1^2 H_{n-2}^1(\alpha_1 r_0)] a_n^{(1)} + [-\alpha_1^2 (\lambda_1 + \mu_1) H_n^2(\alpha_1 r_0) + \mu_1 \alpha_1^2 H_{n-2}^2(\alpha_1 r_0)] c_n^{(1)} + i\mu_1 \beta_1^2 H_{n-2}^1(\beta_1 r_0) b_n^{(1)} + i\mu_1 \beta_1^2 H_{n-2}^2(\beta_1 r_0) d_n^{(1)} = 0, \tag{26}$$

$$[-\alpha_1^2 (\lambda_1 + \mu_1) H_n^1(\alpha_1 r_0) + \mu_1 \alpha_1^2 H_{n+2}^1(\alpha_1 r_0)] a_n^{(1)} + [-\alpha_1^2 (\lambda_1 + \mu_1) H_n^2(\alpha_1 r_0) + \mu_1 \alpha_1^2 H_{n+2}^2(\alpha_1 r_0)] c_n^{(1)} - i\mu_1 \beta_1^2 H_{n+2}^1(\beta_1 r_0) b_n^{(1)} - i\mu_1 \beta_1^2 H_{n+2}^2(\beta_1 r_0) d_n^{(1)} = 0, \tag{27}$$

where  $r_0$  is the radius of the hole, and  $n = 0, \pm 1, \pm 2, \dots, \pm M$ .

On the other hand, the continuous condition at the interface between the rings  $j$  and  $j + 1$  can be expressed as:

$$F_1^{(j)} = -F_1^{(j+1)}, \quad F_2^{(j)} = -F_2^{(j+1)}, \tag{28}$$

$$u_r^{(j)} = u_r^{(j+1)}, \quad v_\theta^{(j)} = v_\theta^{(j+1)}, \tag{29}$$

where  $j = 1, 2, \dots, N$ .

Using Eqs. (16) and (17), Eqs. (28) and (29) can be rewritten as:

$$\begin{aligned}
 & -\alpha_j^2(\lambda_j + \mu_j)\Phi_j(z) + 4\mu_j \frac{\partial^2}{\partial z^2} [\Phi_j(z) + i\Psi_j(z)]e^{2i\theta} \\
 & = -\alpha_{j+1}^2(\lambda_{j+1} + \mu_{j+1})\Phi_{j+1}(z) + 4\mu_{j+1} \frac{\partial^2}{\partial z^2} [\Phi_{j+1}(z) + i\Psi_{j+1}(z)]e^{2i\theta},
 \end{aligned} \tag{30}$$

$$\frac{\partial}{\partial \bar{z}} [\Phi_j(z) - i\Psi_j(z)] = \frac{\partial}{\partial \bar{z}} [\Phi_{j+1}(z) - i\Psi_{j+1}(z)], \tag{31}$$

where  $z = r_j\sigma = r_j e^{i\theta}$ ,  $j = 1, 2, \dots, N$ .

Similarly, substituting Eqs. (21)–(24) into (30) and (31) results in:

$$\begin{aligned}
 & [-\alpha_j^2(\lambda_j + \mu_j)H_n^1(\alpha_j r_j) + \mu_j \alpha_j^2 H_{n-2}^1(\alpha_j r_j)]a_n^{(j)} + [-\alpha_j^2(\lambda_j + \mu_j)H_n^2(\alpha_j r_j) + \mu_j \alpha_j^2 H_{n-2}^2(\alpha_j r_j)]c_n^{(j)} \\
 & \quad + i\mu_j \beta_j^2 H_{n-2}^1(\beta_j r_j)b_n^{(j)} + i\mu_j \beta_j^2 H_{n-2}^2(\beta_j r_j)d_n^{(j)} \\
 & = [-\alpha_{j+1}^2(\lambda_{j+1} + \mu_{j+1})H_n^1(\alpha_{j+1} r_j) + \mu_{j+1} \alpha_{j+1}^2 H_{n-2}^1(\alpha_{j+1} r_j)]a_n^{(j+1)} \\
 & \quad + [-\alpha_{j+1}^2(\lambda_{j+1} + \mu_{j+1})H_n^2(\alpha_{j+1} r_j) + \mu_{j+1} \alpha_{j+1}^2 H_{n-2}^2(\alpha_{j+1} r_j)]c_n^{(j+1)} \\
 & \quad + i\mu_{j+1} \beta_{j+1}^2 H_{n-2}^1(\beta_{j+1} r_j)b_n^{(j+1)} + i\mu_{j+1} \beta_{j+1}^2 H_{n-2}^2(\beta_{j+1} r_j)d_n^{(j+1)},
 \end{aligned} \tag{32}$$

$$\begin{aligned}
 & [-\alpha_j^2(\lambda_j + \mu_j)H_n^1(\alpha_j r_j) + \mu_j \alpha_j^2 H_{n+2}^1(\alpha_j r_j)]a_n^{(j)} + [-\alpha_j^2(\lambda_j + \mu_j)H_n^2(\alpha_j r_j) + \mu_j \alpha_j^2 H_{n+2}^2(\alpha_j r_j)]c_n^{(j)} \\
 & \quad - i\mu_j \beta_j^2 H_{n+2}^1(\beta_j r_j)b_n^{(j)} - i\mu_j \beta_j^2 H_{n+2}^2(\beta_j r_j)d_n^{(j)} \\
 & = [-\alpha_{j+1}^2(\lambda_{j+1} + \mu_{j+1})H_n^1(\alpha_{j+1} r_j) + \mu_{j+1} \alpha_{j+1}^2 H_{n+2}^1(\alpha_{j+1} r_j)]a_n^{(j+1)} \\
 & \quad + [-\alpha_{j+1}^2(\lambda_{j+1} + \mu_{j+1})H_n^2(\alpha_{j+1} r_j) + \mu_{j+1} \alpha_{j+1}^2 H_{n+2}^2(\alpha_{j+1} r_j)]c_n^{(j+1)} \\
 & \quad - i\mu_{j+1} \beta_{j+1}^2 H_{n+2}^1(\beta_{j+1} r_j)b_n^{(j+1)} - i\mu_{j+1} \beta_{j+1}^2 H_{n+2}^2(\beta_{j+1} r_j)d_n^{(j+1)},
 \end{aligned} \tag{33}$$

$$\begin{aligned}
 & \alpha_j H_{n-1}^1(\alpha_j r_j)a_n^{(j)} + \alpha_j H_{n-1}^2(\alpha_j r_j)c_n^{(j)} + i\beta_j H_{n-1}^1(\beta_j r_j)b_n^{(j)} + i\beta_j H_{n-1}^2(\beta_j r_j)d_n^{(j)} \\
 & = \alpha_{j+1} H_{n-1}^1(\alpha_{j+1} r_j)a_n^{(j+1)} + \alpha_{j+1} H_{n-1}^2(\alpha_{j+1} r_j)c_n^{(j+1)} + i\beta_{j+1} H_{n-1}^1(\beta_{j+1} r_j)b_n^{(j+1)} \\
 & \quad + i\beta_{j+1} H_{n-1}^2(\beta_{j+1} r_j)d_n^{(j+1)},
 \end{aligned} \tag{34}$$

$$\begin{aligned}
 & \alpha_j H_{n+1}^1(\alpha_j r_j)a_n^{(j)} + \alpha_j H_{n+1}^2(\alpha_j r_j)c_n^{(j)} - i\beta_j H_{n+1}^1(\beta_j r_j)b_n^{(j)} - i\beta_j H_{n+1}^2(\beta_j r_j)d_n^{(j)} \\
 & = \alpha_{j+1} H_{n+1}^1(\alpha_{j+1} r_j)a_n^{(j+1)} + \alpha_{j+1} H_{n+1}^2(\alpha_{j+1} r_j)c_n^{(j+1)} \\
 & \quad - i\beta_{j+1} H_{n+1}^1(\beta_{j+1} r_j)b_n^{(j+1)} - i\beta_{j+1} H_{n+1}^2(\beta_{j+1} r_j)d_n^{(j+1)},
 \end{aligned} \tag{35}$$

where  $j = 1, 2, \dots, (N - 1)$ , and when  $j = N$  results in:

$$\begin{aligned}
 & [-\alpha_j^2(\lambda_j + \mu_j)H_n^1(\alpha_j r_j) + \mu_j \alpha_j^2 H_{n-2}^1(\alpha_j r_j)]a_n^{(j)} + [-\alpha_j^2(\lambda_j + \mu_j)H_n^2(\alpha_j r_j) + \mu_j \alpha_j^2 H_{n-2}^2(\alpha_j r_j)]c_n^{(j)} \\
 & \quad + i\mu_j \beta_j^2 H_{n-2}^1(\beta_j r_j)b_n^{(j)} + i\mu_j \beta_j^2 H_{n-2}^2(\beta_j r_j)d_n^{(j)} \\
 & = [-\alpha_{j+1}^2(\lambda_{j+1} + \mu_{j+1})H_n^1(\alpha_{j+1} r_j) + \mu_{j+1} \alpha_{j+1}^2 H_{n-2}^1(\alpha_{j+1} r_j)]a_n^{(j+1)} \\
 & \quad + [-\alpha_{j+1}^2(\lambda_{j+1} + \mu_{j+1})J_n(\alpha_{j+1} r_j) + \mu_{j+1} \alpha_{j+1}^2 J_{n-2}(\alpha_{j+1} r_j)]\varphi_0 \cdot i^n \\
 & \quad + i\mu_{j+1} \beta_{j+1}^2 H_{n-2}^1(\beta_{j+1} r_j)b_n^{(j+1)},
 \end{aligned} \tag{36}$$

$$\begin{aligned}
 & [-\alpha_j^2(\lambda_j + \mu_j)H_n^1(\alpha_j r_j) + \mu_j \alpha_j^2 H_{n+2}^1(\alpha_j r_j)]a_n^{(j)} + [-\alpha_j^2(\lambda_j + \mu_j)H_n^2(\alpha_j r_j) + \mu_j \alpha_j^2 H_{n+2}^2(\alpha_j r_j)]c_n^{(j)} \\
 & \quad - i\mu_j \beta_j^2 H_{n+2}^1(\beta_j r_j)b_n^{(j)} - i\mu_j \beta_j^2 H_{n+2}^2(\beta_j r_j)d_n^{(j)} \\
 & = [-\alpha_{j+1}^2(\lambda_{j+1} + \mu_{j+1})H_n^1(\alpha_{j+1} r_j) + \mu_{j+1} \alpha_{j+1}^2 H_{n+2}^1(\alpha_{j+1} r_j)]a_n^{(j+1)} \\
 & \quad + [-\alpha_{j+1}^2(\lambda_{j+1} + \mu_{j+1})J_n(\alpha_{j+1} r_j) + \mu_{j+1} \alpha_{j+1}^2 J_{n+2}(\alpha_{j+1} r_j)]\varphi_0 \cdot i^n \\
 & \quad - i\mu_{j+1} \beta_{j+1}^2 H_{n+2}^1(\beta_{j+1} r_j)b_n^{(j+1)},
 \end{aligned} \tag{37}$$

$$\alpha_j H_{n-1}^1(\alpha_j r_j) a_n^{(j)} + \alpha_j H_{n-1}^2(\alpha_j r_j) c_n^{(j)} + i\beta_j H_{n-1}^1(\beta_j r_j) b_n^{(j)} + i\beta_j H_{n-1}^2(\beta_j r_j) d_n^{(j)} = \alpha_{j+1} H_{n-1}^1(\alpha_{j+1} r_j) a_n^{(j+1)} + \alpha_{j+1} J_{n-1}(\alpha_{j+1} r_j) \varphi_0 \cdot i^n + i\beta_{j+1} H_{n-1}^1(\beta_{j+1} r_j) b_n^{(j+1)}, \tag{38}$$

$$\alpha_j H_{n+1}^1(\alpha_j r_j) a_n^{(j)} + \alpha_j H_{n+1}^2(\alpha_j r_j) c_n^{(j)} - i\beta_j H_{n+1}^1(\beta_j r_j) b_n^{(j)} - i\beta_j H_{n+1}^2(\beta_j r_j) d_n^{(j)} = \alpha_{j+1} H_{n+1}^1(\alpha_{j+1} r_j) a_n^{(j+1)} + \alpha_{j+1} J_{n+1}(\alpha_{j+1} r_j) \varphi_0 \cdot i^n - i\beta_{j+1} H_{n+1}^1(\beta_{j+1} r_j) b_n^{(j+1)}, \tag{39}$$

where  $n = 0, \pm 1, \pm 2, \dots, \pm M$ .

Equations (26), (27) and (32)–(39) constitute a set of  $2(2N + 1)(2M + 1)$  linear equations which contain  $2(2N + 1)(2M + 1)$  unknown coefficients  $a_n^{(j)}, b_n^{(j)}, c_n^{(j)}, d_n^{(j)}$  ( $j = 1, 2, \dots, N; n = 0, \pm 1, \pm 2, \dots, \pm M$ ) and  $a_n^{(N+1)}, b_n^{(N+1)}$ , and thus all these unknown coefficients can be determined by using transfer matrix solution technique. Then, all the complex potentials become known in any ring, and finally field variables in the plate can be approximately determined from Eqs. (14) and (15).

### 4 Numerical examples

Numerical results are obtained in dimensionless forms by normalizing with respect to the stress associated with the incident wave; that is:

$$\sigma_0 = -\mu_{N+1} \beta_{N+1}^2 \varphi_0, \tag{40}$$

The hoop stress around the circular hole is written as:

$$\sigma_\theta^* = \frac{\sigma_\theta}{\sigma_0} = \frac{2(\lambda_1 + \mu_1)\alpha_1^2}{\mu_{N+1}\beta_{N+1}^2\varphi_0} \operatorname{Re} \left\{ \sum_{-\infty}^{+\infty} [a_n^{(1)} H_n^1(\alpha_1 r) + c_n^{(1)} H_n^2(\alpha_1 r)] e^{in\theta} \right\} e^{-i\omega t}. \tag{41}$$

In the following numerical examples, we will discuss the effect of shear modulus  $\mu$ , density  $\rho$  and Poisson’s ratio  $\nu$  on the normalized stress  $\sigma_\theta^*$ , respectively.

Firstly, we check the accuracy of the present numerical analysis by comparing the obtained solutions for several special cases with those given in previous works. For example, consider a homogeneous plate with a circular hole having the material parameters as:

$$\mu(r) = \mu_0, \tag{42}$$

$$\rho(r) = \rho_0, \tag{43}$$

$$\nu(r) = \nu_0, \tag{44}$$

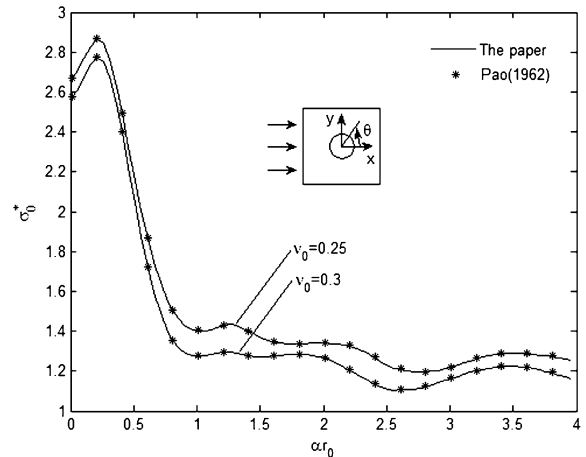


**Fig. 4** Distribution of stress for homogeneous plate with a circular hole ( $r = r_0, \theta = \pi/2$ )

where  $\mu_0, \rho_0$  and  $\nu_0$  is constant. In this case, it is analyzed the normalized hoop stresses at the position of  $\theta = \pi/2$  as a function of dimensionless wave number  $\alpha r_0$  for two Poisson’s ratios;  $\nu_0 = 0.25$  and  $\nu_0 = 0.3$ . The results are shown in Fig. 4 and they agree with those reported in Pao [14].

For another case when the number of layers  $N = 1$ , the results for an infinite elastic medium with a cylindrical lining may be derived. In order to compare the results with that in Mow and McCabe [15], the material parameters for the case of the stiff cylindrical lining are taken as  $\mu_2/\mu_1 = 0.31, C_{\alpha 2}/C_{\alpha 1} = 0.7, \nu_1 = 0.3$  and  $\nu_2 = 0.25$ . The distribution of normalized hoop stresses for  $r_1/r_0 = 1.05, 1.1$  and  $1.2$  are shown in Fig. 5. Compared the results with those in Mow and McCabe [15], the error is about 1 %.

#### 4.1 Effects of variations of shear modulus on the stress

To study the effect of shear modulus on the stress, we take the material shear modulus  $\mu$  as three different situations:

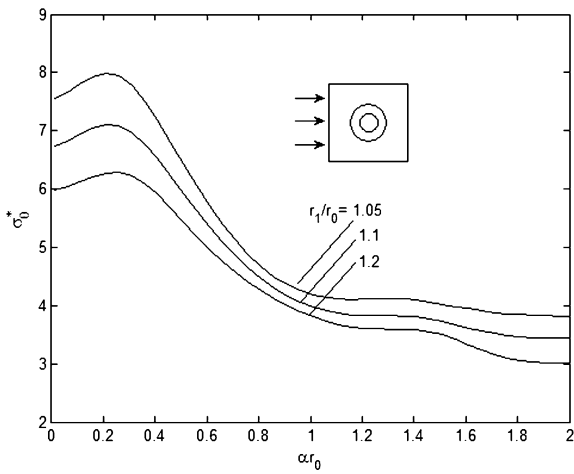


**Fig. 5** Distribution of stress for elastic medium with a cylindrical lining ( $r = r_0, \theta = \pi/2$ )

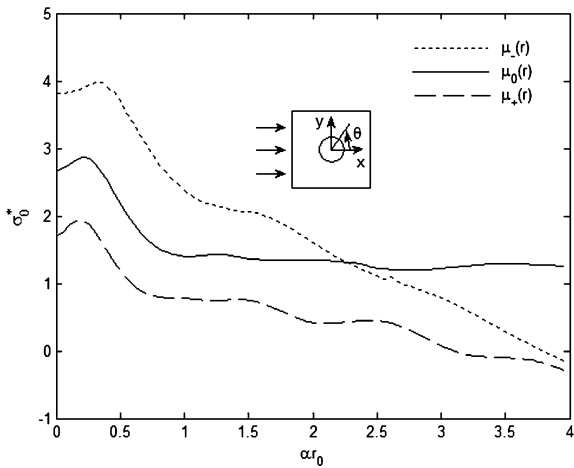


**Fig. 6** Distribution of stress as  $\mu$  changes in different ways ( $r = r_0, \theta = \pi/2$ )

$$\mu_-(r) = 0.5 * \mu_0 \left( 1 + \frac{e}{e^{r/r_0}} \right), \tag{45}$$

$$\mu_0(r) = \mu_0, \tag{46}$$

$$\mu_+(r) = \mu_0 \left( 1 - 0.5 \frac{e}{e^{r/r_0}} \right). \tag{47}$$

In addition, the density  $\rho(r) = \rho_0$  and Poisson's ratio  $\nu(r) = \nu_0 = 0.25$  are taken. In this case, the normalized stress  $\sigma_\theta^*$  as a function of dimensionless wave number  $\alpha r_0$  is shown in Fig. 6. It is found that when the density and Poisson's ratio are kept unchanged, the increase of shear modulus in the radial direction make the stress decreased, while the decrease of shear mod-

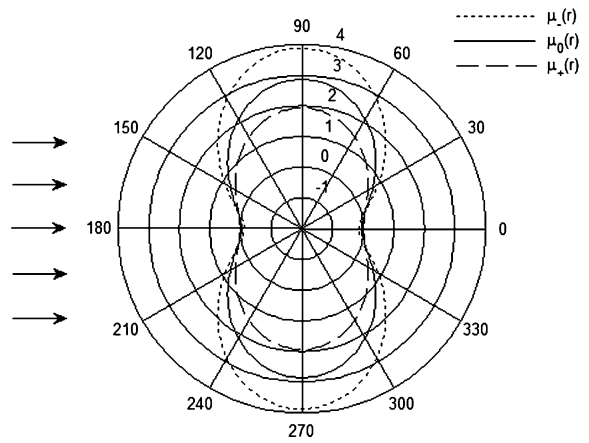


**Fig. 7** Angular distribution of stress  $\sigma_\theta^*$  around the hole as  $\mu$  changes in different ways ( $\alpha r_0 = 0.2$ )

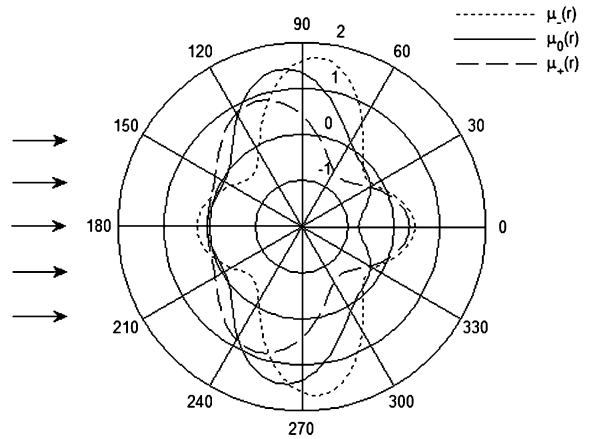


**Fig. 8** Angular distribution of stress  $\sigma_\theta^*$  around the hole as  $\mu$  changes in different ways ( $\alpha r_0 = 2.0$ )

ulus can increase the stress as wave number less than about 2.2.

Figures 7 and 8 show the angular distribution of the stress  $\sigma_\theta^*$  around the hole for two wave numbers;  $\alpha r_0 = 0.2$  and  $\alpha r_0 = 2.0$ . At the low wave number, the stress is not only symmetric with respect to the  $x$ -axis but also approximately symmetric with respect to the  $y$ -axis. As the shear modulus decreases along the radial direction, the stress around the hole obviously increases; on the contrary, as the shear modulus increases, the stress reduces. For a high frequency incident wave with  $\alpha r_0 = 2.0$ , the stress is no longer symmetric with respect to the  $y$ -axis. The peak stress is shifted toward the incident side of the hole for  $\mu_0(r)$  and  $\mu_+(r)$  but toward the other side for  $\mu_-(r)$ . In this

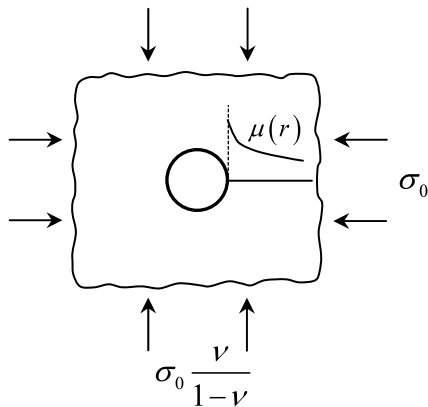


**Fig. 9** FGM plate with a circular hole subjected to biaxial load at infinity

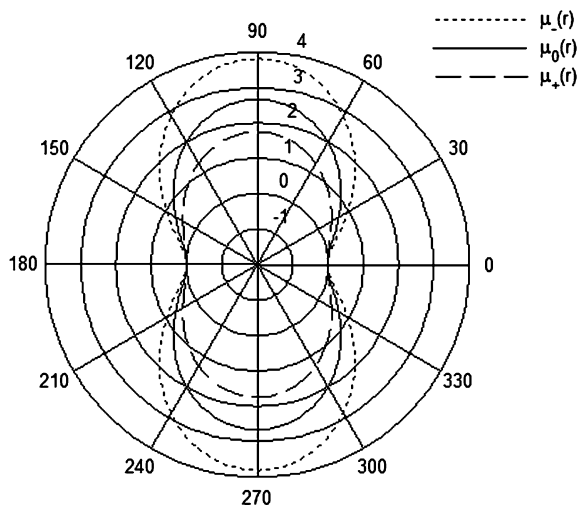


**Fig. 10** Angular distribution of stress  $\sigma_\theta/\sigma_0$  around the hole as  $\mu$  changes in different ways under biaxial load

case, the magnitude of stress is generally lower than that for a low frequency incident wave with  $\alpha r_0 = 0.2$ .

For a special case of incident wave, in which  $\alpha \rightarrow 0$ , the incident wave represents a biaxial loading with  $\sigma_{xx} = -\sigma_0$  and  $\sigma_{yy} = -\sigma_0 \nu / (1 - \nu)$  [27], as shown in Fig. 9. We choose three different variations of shear modulus  $\mu_-(r)$ ,  $\mu_0(r)$  and  $\mu_+(r)$  as shown in Eqs. (45)–(47). In addition, the density and Poisson’s ratio are kept as constant and  $\nu = 0.25$ . With using the method introduced by Yang *et al.* [28], the stress  $\sigma_\theta/\sigma_0$  around the hole is derived and the result is shown in Fig. 10. Compared with Fig. 7, it is found that the stress for the low frequency incident wave with  $\alpha r_0 = 0.2$  is only slightly different from the static so-

**Table 1** The dimensionless dynamic and static stresses at the position of  $\theta = \pi/2$  for three different variations of shear modulus

	$\mu_-(r)$	$\mu_0(r)$	$\mu_+(r)$
Dynamic stress	3.804	2.669	1.743
Static stress	3.817	2.667	1.751

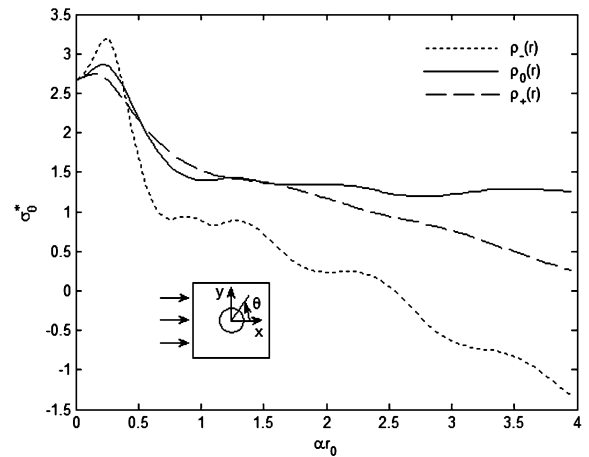


**Fig. 11** Distribution of stress as  $\rho$  changes in different ways ( $r = r_0, \theta = \pi/2$ )

lution. And if a lower wave number is taken, the corresponding result will be closer to the static answer. For example, the dynamic stress at the position of  $\theta = \pi/2$  for wave number  $\alpha r_0 = 0.01$  is calculated and shown in Table 1. Compared with the static stress, it is observed that the results are very close and the error is less than 0.5 %.

4.2 Effects of variations of density on the stress

The density  $\rho$  is taken as three different situations:

$$\rho_-(r) = 0.5 * \rho_0 \left( 1 + \frac{e}{e^{r/r_0}} \right), \tag{48}$$

$$\rho_0(r) = \rho_0, \tag{49}$$

$$\rho_+(r) = \rho_0 \left( 1 - 0.5 \frac{e}{e^{r/r_0}} \right), \tag{50}$$

In addition, the shear modulus  $\mu(r) = \mu_0$  and Poisson’s ratio  $\nu(r) = \nu_0 = 0.25$  are used. In this case, the variation of stress  $\sigma_\theta^*$  with the dimensionless wave number  $\alpha r_0$  is shown in Fig. 11. It can be seen that the change of density influences the stress obviously in the region of high frequency especially for the case



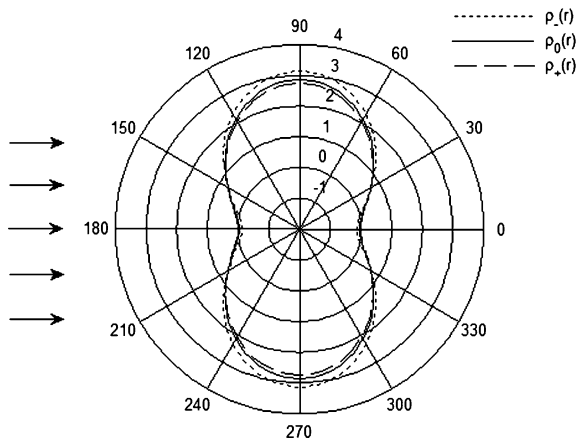


**Fig. 12** Angular distribution of stress  $\sigma_\theta^*$  around the hole as  $\rho$  changes in different ways ( $\alpha r_0 = 0.2$ )

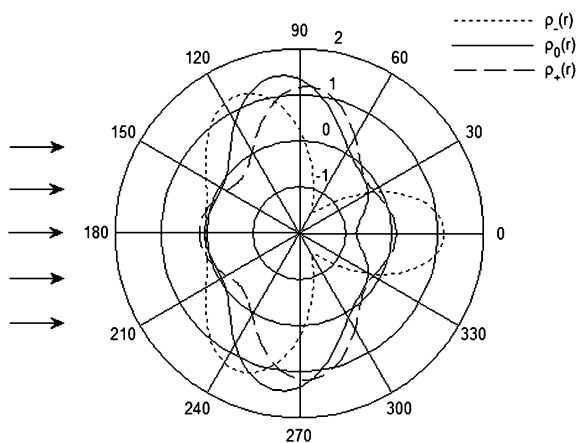


**Fig. 13** Angular distribution of stress  $\sigma_\theta^*$  around the hole as  $\rho$  changes in different ways ( $\alpha r_0 = 2.0$ )

of  $\rho_-(r)$ . As wave number  $\alpha r_0 \rightarrow 0$ , the variation of density has little effect on the stress. That's because the situation of  $\alpha r_0 \rightarrow 0$  can be considered as a static loading condition. In the static state, as we all know, the stress is not influenced by the change of density.

Figures 12 and 13 show the angular distribution of the stress  $\sigma_\theta^*$  around the hole for two wave numbers;  $\alpha r_0 = 0.2$  and  $\alpha r_0 = 2.0$ . At the low wave number, the stress is symmetric with respect to both axes and the influence of the variation of density on the stress is small. For a high frequency incident wave with  $\alpha r_0 = 2.0$ , the peak stress is shifted toward the incident side of the hole for  $\rho_-(r)$  but toward the other side for  $\rho_+(r)$ , which is contrary to the case of shear modulus.

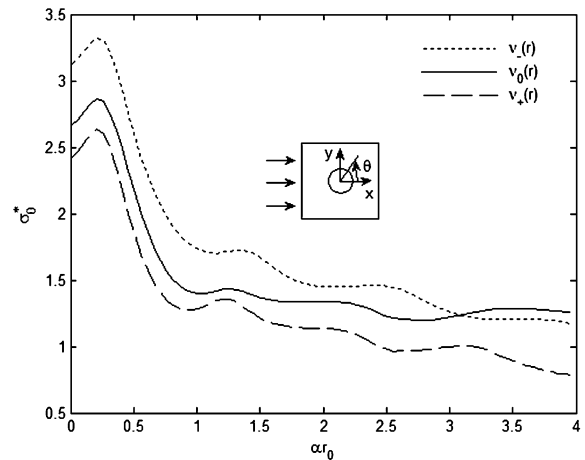


**Fig. 14** Distribution of stress as  $\nu$  changes in different ways ( $r = r_0, \theta = \pi/2$ )

### 4.3 Effects of variations of Poisson's ratio on the stress

Finally, to examine the effects of the material Poisson's ratio  $\nu$ , we take the following three different functions:

$$\nu_-(r) = 0.5 * \nu_0 \left( 1 + \frac{e}{e^{r/r_0}} \right), \tag{51}$$

$$\nu_0(r) = \nu_0, \tag{52}$$

$$\nu_+(r) = \nu_0 \left( 1 - 0.5 \frac{e}{e^{r/r_0}} \right), \tag{53}$$

where  $\nu_0 = 0.25$  and other material properties are kept as constant. In this case, the distribution of normalized stress  $\sigma_\theta^*$  is shown in Fig. 14. It is found that the increase of Poisson's ratio in the radial direction reduces the stress, while the decrease of Poisson's ratio makes the stress increased, except for the case of wave number more than about 3.1.

Figures 15 and 16 show the angular distribution of the stress  $\sigma_\theta^*$  around the hole for two wave numbers;  $\alpha r_0 = 0.2$  and  $\alpha r_0 = 2.0$ . At the low wave number, the effect of Poisson's ratio on the stress is similar to that of shear modulus, but the influence level is relatively lower. For the case of  $\alpha r_0 = 2.0$ , the peak stress is shifted toward the incident side of the hole for all three situations. Moreover, the change of the magnitude of stress is small.

## 5 Conclusions

We studied the two-dimensional problem of dynamical stress distribution in a functionally graded mate-

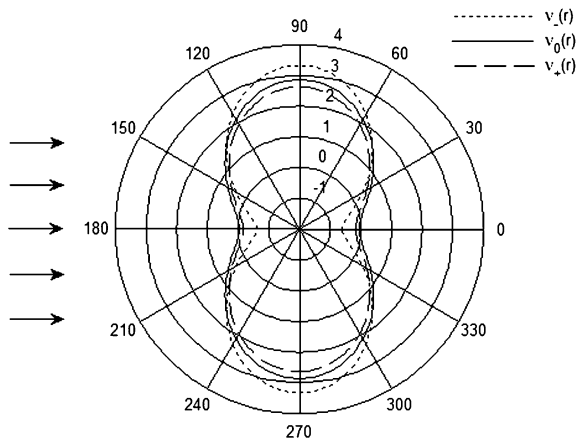


**Fig. 15** Angular distribution of stress  $\sigma_{\theta}^*$  around the hole as  $\nu$  changes in different ways ( $\alpha r_0 = 0.2$ )

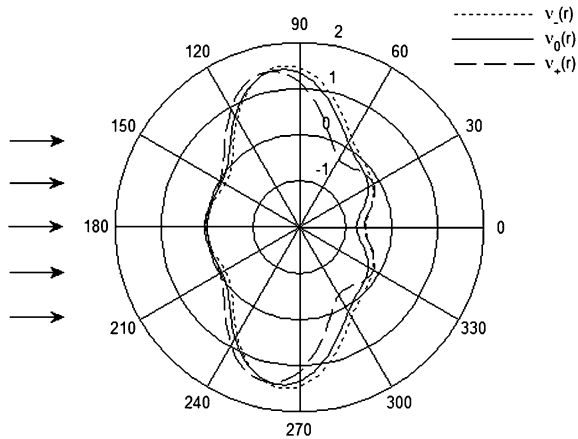


**Fig. 16** Angular distribution of stress  $\sigma_{\theta}^*$  around the hole as  $\nu$  changes in different ways ( $\alpha r_0 = 2.0$ )

rial plate with a circular hole under plane compressional waves at infinity. By using the method of piecewise homogeneous layers, the problem is reduced approximately to the case where the homogeneous material contains  $N$  rings which have different material constants, and thus it can be solved based on the theory of the complex variable functions. Discussions are made about the effects of shear modulus, density and Poisson's ratio on the dynamic stress around the circular hole by numerical examples. It is found that the decrease of shear modulus in the radial direction makes the stress increased for the low frequency incident wave, while decreased for the high frequency incident wave. However, the increase of shear modulus reduces the stress for each frequency incident wave. On the other hand, the change of density influences

the stress obviously only for the high frequency incident wave. Additionally, the effect of Poisson's ratio on the stress is similar to that of shear modulus, but the influence level is relatively lower. Thus, the dynamic stress around the circular hole in the infinite medium can be effectively reduced by choosing the proper change ways of the radial material parameters for different frequency incident wave.

**Acknowledgements** The authors thank the financial support from the National Natural Science Foundation of China (10972103) and the Ph.D. Programs Foundation of Ministry of Education of China (20093218110004). QQY is also grateful to the support of Funding of Jiangsu Innovation Program for Graduate Education (CXZZ11\_0191) and Funding for Outstanding Doctoral Dissertation in NUAA (BCXJ11-03).

## References

1. Ma L, Wu LZ, Guo LC (2002) Dynamic behavior of two collinear anti-plane shear cracks in a functionally graded layer bonded to dissimilar half planes. *Mech Res Commun* 29:207–215
2. Meguid SA, Wang XD, Jiang LY (2002) On the dynamic propagation of a finite crack in functionally graded materials. *Eng Fract Mech* 69:1753–1768
3. Chen J, Liu ZX, Zou ZZ (2003) Electromechanical impact of a crack in a functionally graded piezoelectric medium. *Theor Appl Fract Mech* 39:47–60
4. Song SH, Paulino GH (2006) Dynamic stress intensity factors for homogeneous and smoothly heterogeneous materials using the interaction integral method. *Int J Solids Struct* 43:4830–4866
5. Feng WJ, Su RKL (2006) Dynamic internal crack problem of a functionally graded magneto-electro-elastic strip. *Int J Solids Struct* 43:5196–5216
6. Li YD, Lee KY (2008) Fracture analysis of a weak-discontinuous interface in a symmetrical functionally gradient composite strip loaded by anti-plane impact. *Arch Appl Mech* 78:855–866
7. Peng XL, Li XF (2009) Transient response of the crack-tip field in a magneto-electroelastic half-space with a functionally graded coating under impacts. *Arch Appl Mech* 79:1099–1113
8. Han X, Liu GR, Xi ZC, Lam KY (2002) Characteristics of waves in a functionally graded cylinder. *Int J Numer Methods Eng* 53:653–676
9. Chen WQ, Bian ZG, Lv CF, Ding HJ (2004) 3D free vibration analysis of a functionally graded piezoelectric hollow cylinder filled with compressible fluid. *Int J Solids Struct* 41:947–964
10. Elmaimouni L, Lefebvre JE, Zhang V, Gryba T (2005) Guided waves in radially graded cylinders: a polynomial approach. *NDT E Int* 38:344–353
11. Bagri A, Eslami MR (2007) Analysis of thermoelastic waves in functionally graded hollow spheres based on the Green-Lindsay theory. *J Therm Stresses* 30:1175–1193

12. Asgari M, Akhlaghi M, Hoseini SM (2009) Dynamic analysis of two-dimensional functionally graded thick hollow cylinder with finite length under impact loading. *Acta Mech* 208:163–180
13. Shariyat M, Khaghani M, Lavasani SMH (2010) Nonlinear thermoelasticity, vibration, and stress wave propagation analyses of thick FGM cylinders with temperature-dependent material properties. *Eur J Mech A, Solids* 29:378–391
14. Pao YH (1962) Dynamical stress concentration in an elastic plate. *J Appl Mech* 29:299–305
15. Mow CC, McCabe WL (1963) Dynamic stresses in an elastic cylinder. *Proceedings of the American Society of Civil Engineers, J Eng Mech Div* 89:21–41
16. Liu DK, Gai BZ, Tao GY (1982) Applications of the method of complex function to dynamic stress concentration. *Wave Motion* 4:293–304
17. Shankar K (1998) A study of the dynamic stress concentration factors of a flat plate for sea applications. *J Sound Vib* 217:97–111
18. Altenhof W, Zamani N, North W, Arnold B (2004) Dynamic stress concentrations for an axially loaded strut at discontinuities due to an elliptical hole or double circular notches. *Int J Impact Eng* 30:255–274
19. Zirka AI, Malezhik MP, Chernyshenko IS (2004) Stress concentration in an orthotropic plate with a circular hole under dynamic loading. *Int Appl Mech* 40:226–230
20. Gao SW, Wang YS, Zhang ZM, Ma XR (2005) Dual reciprocity boundary element method for flexural waves in thin plate with cutout. *Appl Math Mech* 26:1564–1573
21. Wang JH, Zhou XL, Lu JF (2005) Dynamic stress concentration around elliptic cavities in saturated poroelastic soil under harmonic plane waves. *Int J Solids Struct* 42:4295–4310
22. Wang GF, Wang TJ, Feng XQ (2006) Surface effects on the diffraction of plane compressional waves by a nanosized circular hole. *Appl Phys Lett* 89:231923
23. Fang XQ, Hu C, Du SY (2006) Strain energy density of a circular cavity buried in semi-infinite functionally graded materials subjected to shear waves. *Theor Appl Fract Mech* 46:166–174
24. Fang XQ, Hu C, Du SY (2007) Dynamic stress of a circular cavity buried in a semi-infinite functionally graded material subjected to shear waves. *J Appl Mech* 74:916–922
25. Fang XQ, Hu C, Huang WH (2007) Strain energy density of a circular cavity buried in a semi-infinite slab of functionally graded materials subjected to anti-plane shear waves. *Int J Solids Struct* 44:6987–6998
26. Dineva P, Gross D, Muller R, Rangelov T (2011) Dynamic stress and electric field concentration in a functionally graded piezoelectric solid with a circular hole. *Z Angew Math Mech* 91:110–124
27. Pao YH, Mow CC (1973) *Diffraction of elastic waves and dynamic stress concentrations*. Crane and Russak, New York
28. Yang QQ, Gao CF, Chen WT (2010) Stress analysis of a functional graded material plate with a circular hole. *Arch Appl Mech* 80:895–907